Chemical Science

ROYAL SOCIETY OF CHEMISTRY

EDGE ARTICLE

View Article Online
View Journal | View Issue

Cite this: *Chem. Sci.*, 2024, **15**, 4590

All publication charges for this article have been paid for by the Royal Society of Chemistry

From π-conjugated macrocycles to heterocycloarenes based on benzo[2,1-*b*:3,4-*b*′] dithiophene (BDTh): size- and geometry-dependent host–guest properties†

Dongyue An, Rong Zhang, Jiangyu Zhu, Teng Wang, Yan Zhao, Xuefeng Lu * and Yunqi Liu

Received 27th September 2023
Accepted 19th February 2024

DOI: 10.1039/d3sc05074b

rsc.li/chemical-science

π-Conjugated macrocycles have been highly attractive due to their challenging synthesis, fascinating aesthetic structure and unique physical and chemical properties. Although some progress has been made in synthesis, the study of π-macrocycles with different structural characteristics and supramolecular interactions still faces major challenges. In this paper, two new single-bond linked macrocycles (**MS-4T**/**MS-6T**) were reported, and the corresponding vinyl-bridged heterocycloarenes (**MF-4T**/**MF-6T**) were synthesized by the periphery fusion strategy. Further studies have indicated that the structure of these four macrocycles is determined by both size and curvature, showing unique variations from nearly planar to bowl and then to saddle. Interestingly, the nearly planar **MS-4T** with a small size and the rigid saddle-shaped **MF-6T** show no obvious response to fullerenes C_{60} or C_{70}, while the bowl-shaped **MS-6T** and **MF-4T** demonstrate a strong binding affinity towards fullerenes C_{60} and C_{70}. What's more, two kinds of co-crystals with capsule-like configurations, **MS-6T**@C_{60} and **MS-6T**@C_{70}, have been successfully obtained, among which the former shows a loose columnar arrangement while the latter displays a unique three-dimensional honeycomb arrangement that is extremely rare in supramolecular complexes. This work systematically studies the π-conjugated macrocycles and provides a new idea for the development of novel host–guest systems and further multifunctional applications.

Introduction

π-Conjugated macrocycles[1] are an important kind of organic conjugated materials with special geometric structures, physicochemical properties and good electron transport characteristics, demonstrating broad application prospects in organic electronic devices,[2] supramolecular assembly[3] and chemical sensors.[4] They can be roughly divided into single bond linked macrocycles and fully fused cycloarenes according to different structural characteristics. Among them, the single bond linked macrocycles have an inner cavity formed by single bonds and aromatic rings[5] or double[6]/triple[7] bonds, while fully fused cycloarenes[8] have clear internal and external rings constructed by aromatic rings with common edges. Their geometric configurations, optoelectronic properties as well as supramolecular assembly behaviours can be controlled by adjusting the building blocks and conjugation length of π-conjugated systems. [*n*]Cyclo-*meta*-phenylene[9] (CMP) is a kind of typical single bond linked macrocycle whose structure and optoelectronic properties are closely related to the number of phenylene blocks. In fact, for [6]CMP, if we assume that it can be fully periphery-fused, the basic cycloarene kekulene[10] can be obtained, which is composed of 12 benzenoid rings prepared by Stab and Diederich in 1978. And more than 30 years later, septulene[11] with 14 benzenoid rings and octulene[12] with 16 benzenoid rings were successfully synthesized. The conjugated extension significantly transforms these cycloarenes from a planar structure (kekulene) into a twisted saddle structure (octulene), and their supramolecular assembly properties are quite different.[13] In addition to conjugate extension, the introduction of heteroatoms can also greatly change the various properties of macrocycles, as it is conducive to enhancing intramolecular charge transfer, which has a great influence on photophysical and electrochemical properties, as well as device performance. For single bond linked macrocycles, aromatic heterocycles[14] can be used as building blocks, such as thiophene,[15] pyridine,[16] pyrazine,[17] *etc.* Heteroatoms containing lone electron pairs can also be used directly as bridging units to realize the heteroatomization of macrocycles and achieve the

Department of Materials Science, State Key Laboratory of Molecular Engineering of Polymers, Fudan University, Shanghai 200433, China. E-mail: luxf@fudan.edu.cn

† Electronic supplementary information (ESI) available. CCDC 2272202, 2272207, 2327360 and 2272225. For ESI and crystallographic data in CIF or other electronic format see DOI: https://doi.org/10.1039/d3sc05074b

purpose of regulating the performance of the final π-conjugated macrocycles.[18] For fully fused cycloarenes, heteroatoms are generally introduced through aromatic heterocycles.[19] At present, some heterocycloarenes that fuse thiophene,[2e] carbazole[20] and other aromatic heterocycles[21] have been successfully synthesized and show great application prospects in organic optoelectronic devices and supramolecular chemistry.

However, due to the internal strain caused by special topological structures, the accurate construction of π-conjugated macrocycles is not an easy task. What's more, we have found that periphery fusion to build a vinyl bridge for macrocycles and the relationship between single bond linked macrocycles and fully fused cycloarenes have been less investigated. The effect of periphery fusion on the geometrical structure, physicochemical properties and supramolecular assembly behaviours of macrocycles is still an open question. Herein, we report a nearly planar single bond linked π-conjugated macrocycle **MS-4T** and a bowl-shaped macrocycle **MS-6T**, both of which are composed of benzo[2,1-*b*:3,4-*b*′]dithiophene (BDTh) and phenanthrene (Phen) units. In order to further study the effect of periphery fusion on macrocycles, the bowl-shaped heterocycloarene **MF-4T** and saddle-shaped heterocycloarene **MF-6T** on the basis of a single bond linked macrocycle are subsequently synthesized. Thus, the electronic structure, aromaticity, as well as optoelectronic properties of both the single bond linked π-conjugated macrocycles **MS-4T**/**MS-6T** and heterocycloarenes **MF-4T**/**MF-6T** are of great interest. In addition, such types of π-conjugated macrocycles may show selective host–guest interactions with fullerenes. In this article, we will report the synthesis, geometric configurations, optoelectronic properties and selective supramolecular interactions with fullerenes of these single bond linked π-conjugated macrocycles and fully fused heterocycloarenes (Fig. 1).

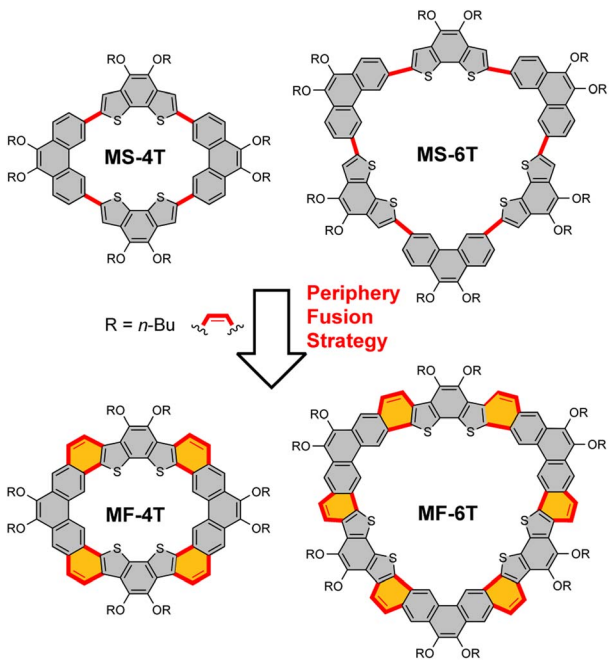

Fig. 1 The design of single bond linked macrocycles and corresponding vinyl-bridged heterocycloarenes.

Results and discussion

Synthetic procedures

The nearly planar single bond linked π-conjugated macrocycle **MS-4T**, bowl-shaped macrocycle **MS-6T**, bowl-shaped heterocycloarene **MF-4T** and saddle-shaped hetero-cycloarene **MF-6T** were synthesized according to Scheme 1. The Suzuki coupling reaction between equimolar amounts of **1** (see synthesis in the ESI†) and **2** (ref. 22) under optimal conditions gave a mixture of **MS-4T** and **MS-6T**, which were further purified by recycling preparative gel permeation chromatography (GPC) with yields of 14% and 8%, respectively.

In order to achieve the fused cyclization of single bond linked π-conjugated macrocycles, compounds **1** and **3**[23] were used for the Suzuki coupling reaction, and the macrocyclic intermediates **4a** and **4b** with four and six aldehyde groups were synthesized. It should be noted that although GPC did not show two distinct product peaks, the single peak was maldistributed (Fig. S7†), indicating that the product was actually a mixture, which was very hard to further separate completely. In addition,

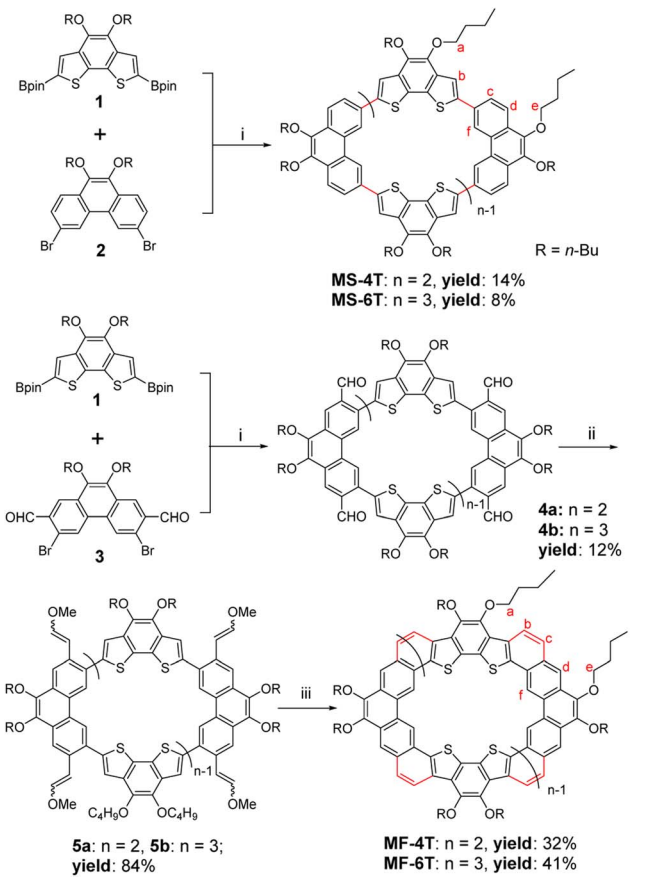

Scheme 1 Synthetic route for the single bond linked macrocycles **MS-4T**/**MS-6T** and heterocycloarenes **MF-4T**/**MF-6T**. (i) XPhos Pd G2, K_3PO_4, THF/H_2O, 60 °C; (ii) methoxymethyltriphenyl-phosphonium chloride, *t*-BuOK, THF, RT; (iii) $Bi(OTf)_3$, $ClCH_2CH_2Cl$, RT.

two peaks of different molecular weight appeared in the MALDI-TOF mass spectrum (Fig. S51 and 52†), corresponding to **4a** and **4b** respectively. The yield of the mixture of **4a** and **4b** was about 18%. Then, the aldehyde groups in the intermediates **4a** and **4b** were converted to methoxyethenyl groups by a Wittig reaction to obtain the corresponding macrocyclic precursors **5a** and **5b** with four and six vinyl ether groups. Similar to the macrocyclic intermediates **4a** and **4b**, **5a** and **5b** were also hard to isolate, and the yield of the mixture of **5a** and **5b** was about 84%. Finally, the periphery fusion of macrocyclic precursors **5a** and **5b** was realized by the Friedel–Crafts reaction catalyzed by $Bi(OTf)_3$ in 1,2-dichloroethane at room temperature, which afforded the expected fully fused heterocycloarenes **MF-4T** and **MF-6T**. The large size difference between the two molecules allowed them to be easily separated by recycling preparative gel permeation chromatography (GPC) with yields of 32% and 37% respectively. All new products were confirmed using $^{1}H/^{13}C$ NMR and mass spectra (see the ESI†).

Ground-state geometry

Single crystals of **MS-4T** were obtained as yellow needle-shaped crystals by slow diffusion of methanol into the chloroform solution under ambient conditions. X-ray crystallography reveals that **MS-4T** adopts a nearly planar structure, in which the two benzo[2,1-*b*:3,4-*b*′]dithiophene (BDTh) building blocks twist slightly out of the plane of phenanthrene (Phen) blocks in opposite directions with a dihedral angle of 14.2°. The long axial length of the inner cavity of **MS-4T** is 11.30 Å and the short axial length is 5.26 Å (Fig. 2a). It is worth noting that **MS-4T** exhibits polymorphism and the configuration of the conjugated skeleton is varied in the same unit cell. As is shown in Fig. 4a, there are nine macrocycles distributed in parallel along the body diagonal of the unit cell, which are centrosymmetric with respect to the central molecule. A detailed crystallographic analysis reveals that the central molecule has a standard symmetrical structure (Fig. 2a), while the other eight molecules exhibit four kinds of conformations (Fig. 3) with different degrees of distortion, in which the dihedral angle between phenanthrene (Phen) blocks varies from 2.2° to 10.1° and the dihedral angle between benzo[2,1-*b*:3,4-*b*′]dithiophene (BDTh) blocks varies from 3.0° to 21.6°.

In addition, the size of the inner cavity of **MS-4T** also changes slightly. The long axial length increases from 11.28 Å to 11.34 Å, while the short axial length decreases from 5.29 Å to 5.16 Å. The

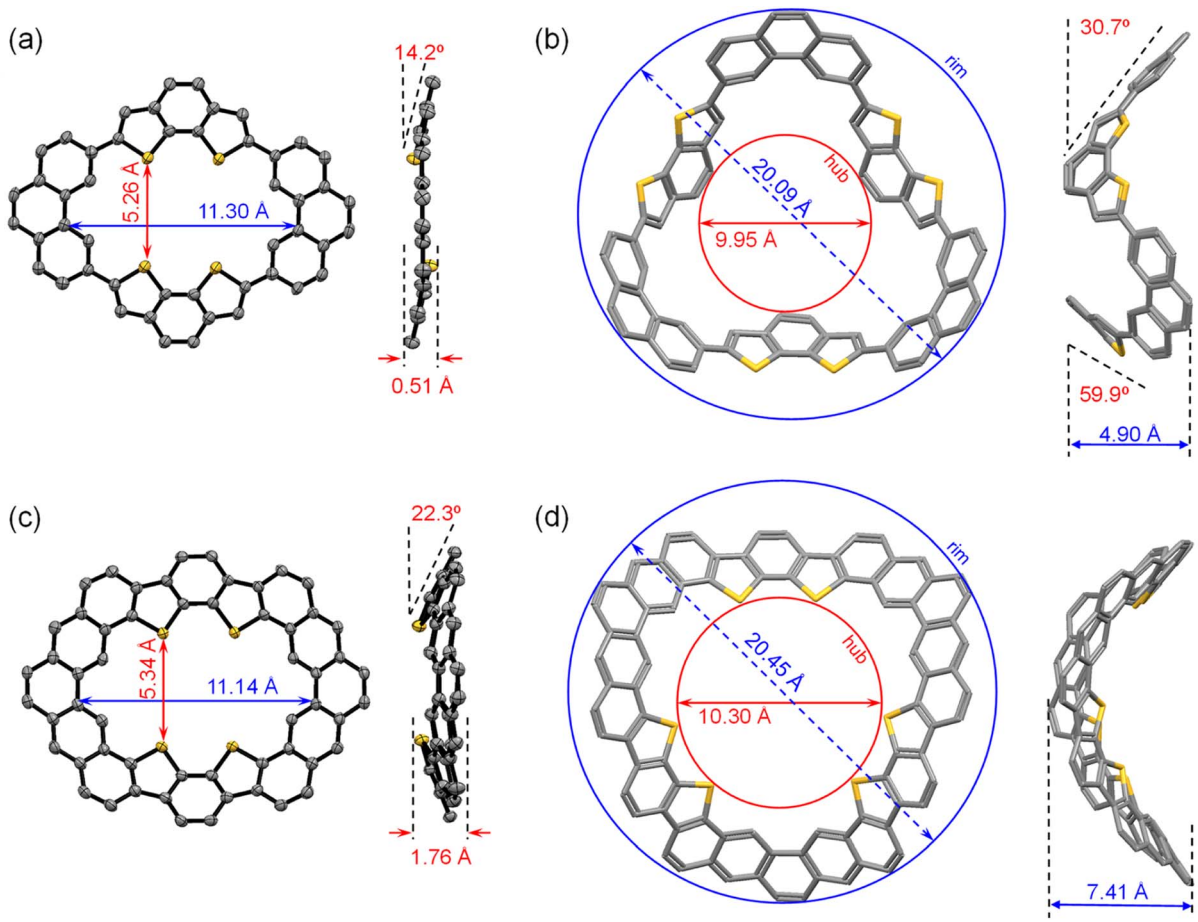

Fig. 2 Top view and side view of the single bond linked macrocycles and heterocycloarenes: (a) X-ray crystallographic structure of **MS-4T** (the ball and stick model); (b) optimized (B3LYP/6-31G(d,p)) structure of **MS-6T** (the capped stick model); (c) X-ray crystallographic structure of **MF-4T** (the ball and stick model); (d) optimized (B3LYP/6-31G(d,p)) structure of **MF-6T** (the capped stick model). All substituents are omitted for clarity.

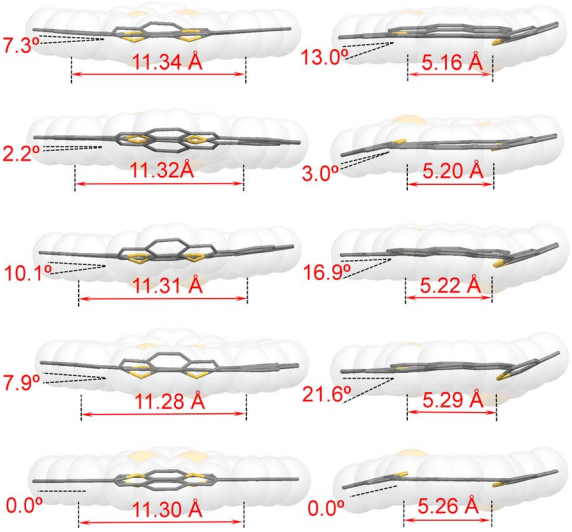

Fig. 3 Five kinds of different crystal structures of polymorphs of MS-4T, with the main view on the left and the corresponding side view on the right. All alkyl chains have been omitted.

π–π distance between two adjacent molecules is 2.84/2.57/2.67/2.66 Å (Fig. 4a) and **MS-4T** molecules pack along the body diagonal of the cell to form columnar stacking with the spacing of layers and columns being 3.52 A and 3.66 A, respectively (Fig. 4a and b). This rare nonamer structure may be related to the tight arrangement of **MS-4T** in the solid phase due to the existence of flexible single bonds, promoting multiple configuration changes to achieve the densest stacking in long-range space. To further study the aromaticity, harmonic oscillator model of aromaticity (HOMA)[38] value calculation was performed on **MS-4T**, which was a method to measure aromaticity based on the geometric structure. The closer HOMA is to 1, the stronger the aromaticity is. If HOMA approaches 0, it is non-aromatic. If it is negative, the bond length is extremely unbalanced, reflecting the anti-aromatic characteristics. According to the results of HOMA value calculations on individual rings, the benzenes on the side of phenanthrene blocks have a larger HOMA value (0.86) than the middle benzenes (0.47). And for the benzo[2,1-*b*:3,4-*b*′]dithiophene (BDTh) blocks, the HOMA value of benzenes (0.85) is larger than that of thiophene (0.57). All the calculation results of macrocycle **MS-4T** are consistent with those of monomers, implying that the formation of the single bond linked π-conjugated macrocycle does not change the aromaticity of each construction unit.

The single crystals of **MS-6T** were also obtained and tested by SC-XRD. However, due to the weak diffraction and complex stacking of the crystal, the structure analysis could not be carried out accurately. Alternatively, the structure of **MS-6T** was optimized by DFT at the B3LYP/6-31G(d,p) level of theory (Fig. 2b). With the increase of building blocks, the geometrical configurations of macrocycles change significantly. According to DFT calculations, **MS-6T** adopts a bowl-shaped structure, in which the diameter of the inner hub and the outer rim is about 9.95 Å and 20.09 Å, respectively. The depth of the bowl can also be obtained by measuring the distance between the mean planes of the inner hub and the outer rim, which is accurate to 4.90 Å. In addition, the sidewall composed of Phen blocks and the opposite sidewall composed of BDTh blocks are tilted about 30.7° and 59.9° relative to the mean plane of the inner rim, respectively. Noticeably, in contrast to **MS-4T**, the BDTh units in **MS-6T** are reversed, with the sulfur atoms oriented toward the outer rim, which may be due to large strain caused by the special bowl-shaped structure. To further verify this change, **MS-4T** and **MS-6T** were tested using 2D NOESY NMR spectra

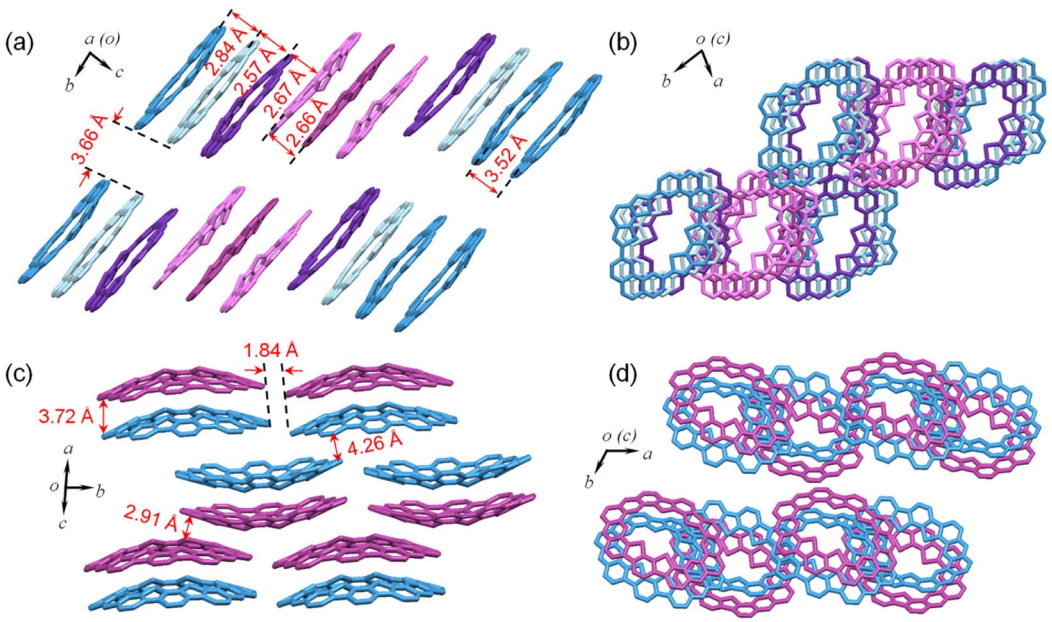

Fig. 4 3D packing structures for MS-4T: (a) side view, (b) top view and MF-4T: (c) side view, (d) top view.

which can reveal the spatial proximity relationship between all protons and protons within the molecule and all aromatic protons have been assigned well. As is shown in Fig. S9,† for **MS-4T**, there is no obvious correlation between the inner-hub proton f and the outer-rim proton b, indicating that the two are far apart in space. But in **MS-6T**, there is a significant correlation between the proton f and b (Fig. S10†), so it can be inferred that BDTh blocks of **MS-6T** are actually flipped relative to the structural formula shown in Scheme 1, which is also consistent with the results of our DFT calculations. In addition, bond length analysis and HOMA value calculations of **MS-6T** are similar to those of **MS-4T**.

To study the effect of periphery fusion on the macrocyclic molecular structure, single crystals of **MF-4T** were obtained as yellow rhombic crystals by slow diffusion of methanol into the toluene solution. As is shown in Fig. 2c, **MF-4T** adopts a bowl-shaped structure with an approximately rectangular inner cavity, in which the long axial length and the short axial length of the inner cavity are about 11.14 Å and 5.34 Å. The bowl depth of **MF-4T** is 1.76 Å, and the side-wall plane is tilted about 22.3° relative to the mean plane containing four sulfur atoms. Interestingly, **MF-4T** exists in the form of a bilayer dimer with the π–π stacking distance of 3.72 Å. The molecules are packed into a unique bilayer-wavy layer stacking due to the bowl-shaped conformation and the distance of two adjacent "waves" formed by dimers is 1.84 Å. The distance of close π–π contacts between the slipped layer molecules is measured to be 2.91 and 4.26 Å respectively (Fig. 4c and d). To further study the new six-membered rings constructed by periphery fusion, bond length analysis and harmonic oscillator model of aromaticity (HOMA) value calculations on individual rings were performed (Fig. S8†). In the hexagons fused from vinyl ethers, the bonds linking the BDTh units and the bonds linking the Phen units (1.43 Å (5)) are close to the typical C(sp^2)–C(sp^2) single bond (1.45 Å), while the bond b (1.37 Å (5)) along the outer periphery is slightly shorter than that of a typical C(sp^2)–C(sp^2) double bond in benzene (1.39 Å). The HOMA value calculations suggest that the newly constructed six-membered rings of **MF-4T** exhibit strong aromatic character (large HOMA values), while the HOMA values of the middle benzene in Phen units decrease significantly compared with **MS-4T**, indicating that the periphery fusion has significantly changed the aromatic properties of the macrocycles. We also tried many methods to grow the single crystals of heterocycloarene **MF-6T** but did not succeed, and the structure of **MF-6T** was optimized by DFT calculations at the B3LYP/6-31G(d,p) level of theory (Fig. 2d). According to DFT calculations, **MF-6T** adopts the shape of a very deep saddle with a maximum bending depth of 7.41 Å, and the inner hub and the outer rim diameters of 10.30 Å and 20.45 Å respectively. In contrast to the sulfur atoms in **MS-6T**, which are oriented toward the outer edge of the bowl-shaped molecule, the sulfur atoms in **MF-6T** are oriented toward the inner edge of the heterocycloarene to realize the periphery fusion of the macrocycle, resulting in its distorted saddle-shaped structure. It was also verified using 2D NOESY NMR spectra (Fig. S14†). Bond length analysis and HOMA value calculations imply that **MF-6T** has a local aromatic character, which is similar to that of **MF-4T**.

Optical and electrochemical properties

Both **MS-4T** and **MS-6T** are yellowish in the solid state, while **MF-4T** and **MF-6T** are deep yellow to yellowish-brown. These four compounds all have good solubility and can be dissolved in common organic solvents, such as toluene, tetrahydrofuran and chloroform, with the solubility varying between 50 and 70 mg ml^{-1}. The absorption spectra and normalized fluorescence emission spectra of **MS-4T**, **MS-6T**, **MF-4T** and **MF-6T** in toluene (*ca.* 10^{-5} M) are shown in Fig. 5. Compounds **MS-4T** and **MS-6T** display intense absorption bands with peaks at 356 and 358 nm respectively, which can be mainly attributed to a combination of HOMO−m → LUMO and HOMO → LUMO+n electronic transitions.[24] **MF-4T** shows a major absorption with maximum wavelength (λ_{max}) at 338 nm and several vibrational peaks in the 350−450 nm region, while **MF-6T** displays a maximum absorption peak at 339 nm with two vibronic shoulders at 324 and 353 nm and several weaker peaks in the 370−450 nm region. The strong absorption in the high energy region can be attributed to a combination of HOMO-m → LUMO and HOMO → LUMO+n electronic transitions, while the lowest absorption band can be attributed to HOMO → LUMO transitions, which is

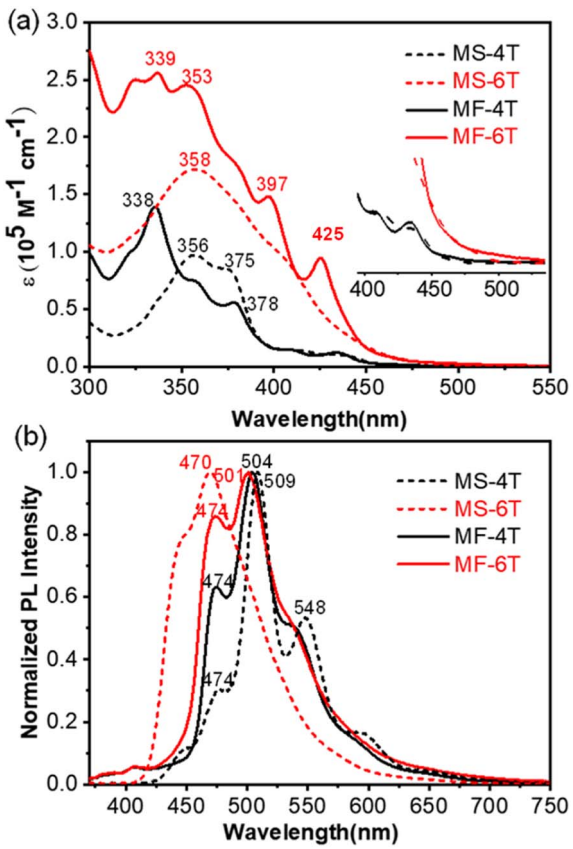

Fig. 5 (a) UV-vis spectra and (b) normalized fluorescence emission spectra of MS-4T, MS-6T, MF-4T and MF-6T in toluene solution; insets show the magnified onset absorption bands.

remarkably similar to that observed in cycloarenes[25] and heterocycloarenes.[3c] The absorption onsets (λ_{onset}) of the four compounds have also been estimated to be 450 nm for **MS-4T**, 463 nm for **MS-6T**, 452 nm for **MF-4T** and 466 nm for **MF-6T**. This slight difference may be the result of a combination of the extension of the π-conjugated system and the twisted geometry of the molecule.[3b,e] According to the lowest-energy absorption onset, the optical energy gap (E_g^{opt}) was estimated to be 2.73 eV, 2.68 eV, 2.74 eV, and 2.66 eV for **MS-4T**, **MS-6T**, **MF-4T** and **MF-6T** respectively.

The normalized fluorescence emission spectra show that the maximum emission wavelength (λ_{em}) of **MS-4T**, **MF-4T** and **MF-6T** is 509 nm, 504 nm, and 501 nm respectively. These similar peaks can be explained by the fact that the redshift caused by extended π-conjugation is offset to some extent by the negative effect of the distorted geometry. However, the fluorescence emission spectra show a significantly blue-shifted maximum emission wavelength (λ_{em} = 470 nm) for **MS-6T** compared with **MS-4T** (λ_{em} = 509 nm), indicating that the Stokes shift of **MS-6T** and the energy loss from the excited state back to the ground state are small. In addition, cyclic voltammetry measurements of **MS-4T**, **MS-6T**, **MF-4T** and **MF-6T** in dry DCM (Fig. S13†) generally revealed multiple irreversible redox waves, which can also be observed in many expanded kekulenes and polycyclic aromatic hydrocarbons containing thiophenes.[26] **MS-4T**, **MS-6T**, **MF-4T** and **MF-6T** exhibit several similar oxidation peaks with initial oxidation potentials at 0.94 V, 0.62 V, 0.73 V and 0.69 V (*vs.* Fc^+/Fc), respectively.

Theoretical calculations

In order to further evaluate the electronic properties of single bond linked π-conjugated macrocycles and fully fused heterocycloarenes, density functional theory (DFT) calculations were conducted by the B3LYP method and 6-31G(d,p) basis set. The calculations were minimized by substituting methyl groups for alkyl chains. As shown in Fig. 6, the frontier HOMO and LUMO coefficients of the nearly planar **MS-4T** and bowl-shaped **MF-4T** are well delocalized along the whole conjugated backbone, which is conducive to intramolecular charge transfer. However, the bowl-shaped **MS-6T** shows two nearly degenerated HOMO and LUMO, with coefficients distributed in half of the molecule. And the saddle-shaped **MF-6T** also shows similar electron cloud distribution in which the HOMO and LUMO are mainly distributed at half of the molecule. The special distributions in **MS-6T** and **MF-6T** can be attributed to their twisted geometric configuration. In addition, the distribution of HOMOs is obvious on the inner and outer edges of the middle benzene rings of Phens in the single bond linked π-conjugated macrocycles **MS-4T**/**MS-6T**. In contrast, the distribution of HOMOs is more obvious on the outer edges but negligible on the inner edges of the middle benzene rings of Phens in the heterocycloarene **MF-4T**/**MF-6T**, suggesting that the periphery fusion may affect the charge distribution on the π-conjugated backbones. What's more, the HOMO and LUMO energy levels of these four macrocycles can be obtained by DFT calculations, from which the energy gaps can also be calculated (Fig. 6). In general, the energy gaps of **MS-4T**, **MF-4T** and **MF-6T** gradually decrease with the increase of size and conjugation degree, which is consistent with the trend of optical band gaps measured from the UV-vis absorption spectrum (Fig. 5a). However, the energy gap of **MS-6T** calculated by DFT theory is quite different from the optical band gap measured by UV-vis absorption spectroscopy, which may be due to the distorted geometry constructed through flexible single bonds.

The ^{1}H NMR spectra (Fig. 7) depict the chemical shifts of the four macrocycles, while calculations were conducted at B3LYP/6-31G(d,p) levels to determine the anisotropy of the induced

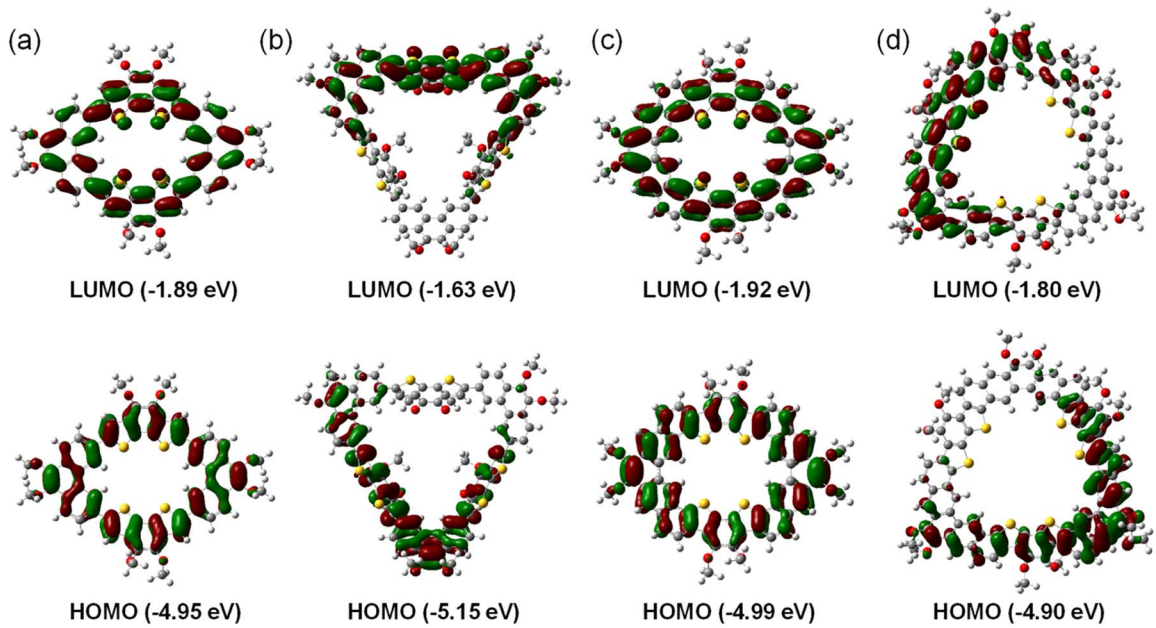

Fig. 6 Calculated frontier molecular orbital profiles (isovalue = 0.02) of the macrocycles: (a) MS-4T, (b) MS-6T, (c) MF-4T, and (d) MF-6T.

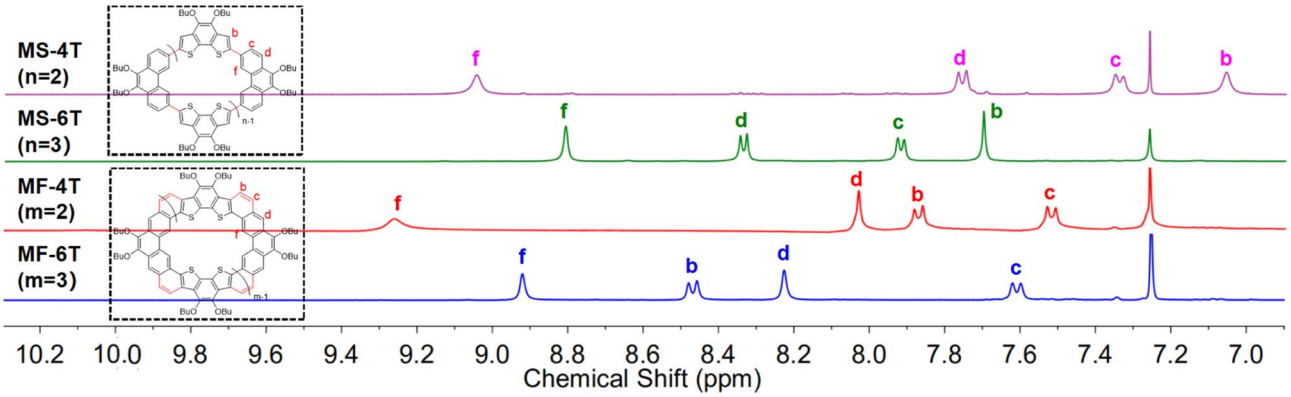

Fig. 7 ^{1}H NMR spectra (aromatic region) of **MS-4T**, **MS-6T**, **MF-4T** and **MF-6T** in CD_3Cl. The small diagrams on the left show the connection modes of building blocks of the macrocycles, and all the protons have been clearly labelled.

current density (ACID)[27] and nucleus independent chemical shift (NICS).[28] As shown in Fig. 8, **MS-4T** and **MS-6T** exhibit four and six local clockwise ring current flows respectively, while the C(sp^2)–C(sp^2) bonds formed by the Suzuki reaction show no ring current flows, which are consistent with the results of bond length analysis, indicating that the single bond linked π-conjugated macrocycles **MS-4T** and **MS-6T** have local aromatic characteristics. The NICS (0) values for **MS-4T** and **MS-6T** are −1.60 and 1.02 ppm respectively. What's more, ACID plots reveal that **MF-4T** and **MF-6T** show local aromatic characteristics and the NICS (0) values are −0.91 and −1.30 ppm respectively, which are similar to the single bond linked π-conjugated macrocycles. However, the distributions of ring current flows in fully fused heterocycloarenes have changed significantly. As shown in Fig. 8, both the C(sp^2)–C(sp^2) bonds formed by the Suzuki reaction and the hexagons fused from vinyl ethers all show heavy ring current, implying obvious aromatic characteristics, which are also reflected in bond length analysis and HOMA value calculations. In addition, compared with typical cycloarenes of the carbon conjugated framework,[25] ring current flows over the C(sp^2)–C(sp^2) double bonds at each corner of **MF-4T**/**MF-6T** can be observed in all cases (seen in Fig. S18–S21 in the ESI†), indicating that the introduction of sulfur atoms significantly changes the distribution of ring current and the aromatization of local rings in heterocycloarenes.

Binding behaviour with fullerenes

Considering that both the single bond linked π-conjugated macrocycles **MS-4T**/**MS-6T** and fully fused heterocycloarenes **MF-4T**/**MF-6T** have well-defined cavities, they may behave as hosts for some typical guests such as fullerenes.[3a,e] Therefore, C_{60} was dropped into the solution of **MS-4T**, **MS-6T**, **MF-4T** and **MF-6T** respectively and then tested using the ^{1}H NMR spectrum at 298 K, in which the feasibility of macrocycles as host molecules was judged by the movement of characteristic peaks.[29] The specific procedure of ^{1}H NMR titration can be seen in the ESI.† For the single bond-linked conjugated macrocycles, no appreciable change was observed when **MS-4T** was mixed with C_{60}, indicating that there was no obvious supramolecular binding[30] (Figure S26a†). However, the mixture of **MS-6T** and C_{60} displayed unusual changes. As shown in Fig. 9a, upon addition of 0.3 equivalent C_{60} to **MS-6T** in CD_2Cl_2, two sets of resonances for the protons of macrocycles appeared in the ^{1}H NMR spectrum, implying a slow-exchange complexation[21,31] between the host **MS-6T** and the guest C_{60}. Affected by the ring currents of aromatic surfaces of spherical C_{60}, the inner hub protons (b and

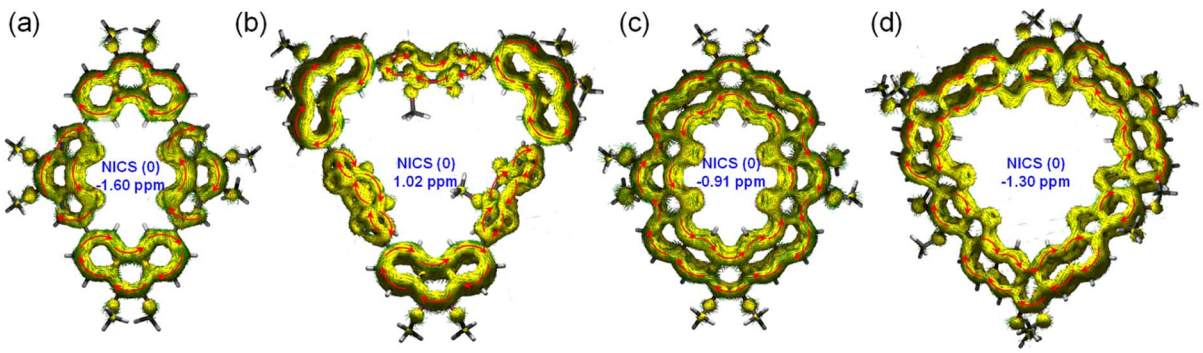

Fig. 8 Calculated ACID plots (contribution from π electrons only) of (a) **MS-4T**, (b) **MS-6T**, (c) **MF-4T** and (d) **MF-6T** with an isovalue of 0.026. The magnetic field is perpendicular to the *XY* plane and points out through the paper. The red arrows indicate clockwise (diamagnetic) current flow.

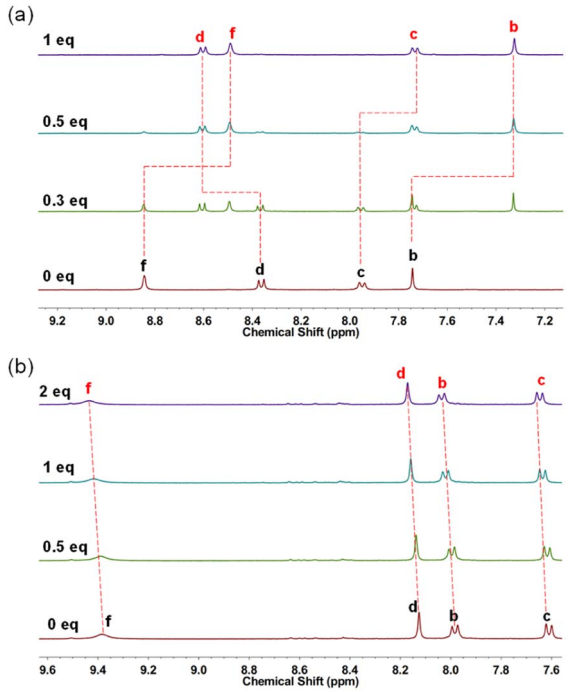

Fig. 9 ^{1}H NMR spectral change of (a) **MS-6T** (in CD_2Cl_2, 1.0 mM) and (b) **MF-4T** (in $CDCl_3$, 1.0 mM) with the addition of C_{60} (in the same solvent with host, 8.0 mM) at 298 K.

f) and the outer rim protons (c) all were shifted to high field, while the outer-most rim protons (d) were shifted to low field, which had been confirmed by 2D NOESY NMR spectroscopy (Fig. S11†). After the addition of C_{60} to half an equivalent of **MS-6T**, the proton signals of free **MS-6T** disappeared while the four new groups of proton signals remained and the integration ratio of the four characteristic peaks was 1 : 1 : 1 : 1. Then no further spectral changes were observed even with increased amounts of C_{60}, indicating that the binding stoichiometry between **MS-6T** and C_{60} tended to be 2 : 1, which was further confirmed by subsequent fluorescence titration tests (Fig. S28 and 29†).

On the other hand, a completely different phenomenon occurred when C_{60} was dropped into the solution of the fully fused heterocycloarenes **MF-4T** and **MF-6T**. With the increase of C_{60}, the aromatic proton signals of **MF-4T** shifted to the downfield and the signal peak of the inner hub proton f widened significantly (Fig. 9b), indicating that there is an obvious supramolecular interaction between the host **MF-4T** and guest C_{60}. In contrast, the trimer heterocycloarene **MF-6T** exhibited no pronounced chemical shift changes, implying that **MF-6T** didn't bind with C_{60} effectively (Fig. S26b†). These entirely different supramolecular binding behaviours can be attributed to the different sizes and geometry of the four macrocycles. For the single bond-linked conjugated macrocycles, the rigid and nearly planar configuration prevents **MS-4T** from effectively encapsulating spherical C_{60} molecules, while **MS-6T** which has a flexible bowl-shaped structure and a large internal cavity can bind with C_{60} strongly. However, after the periphery fusion, it is found that the dimer heterocycloarene **MF-4T** has become a bowl-shaped configuration which is conducive to its binding with C_{60}, while the trimer heterocycloarene **MF-6T** adopts a rigid and highly twisted saddle-shaped structure that no longer has the ability to encapsulate C_{60}. In addition, the ellipsoidal C_{70} was also added to the solution of the four macrocycles as guest molecules, and their supramolecular binding behaviors were similar to those of C_{60} (Fig. S27†).

In addition to the ^{1}H NMR titration spectra, fluorescence titration spectra have also been obtained and the supramolecular assembly properties of hosts (**MS-6T** and **MF-4T**) and guests (C_{60} and C_{70}) in toluene were quantitatively analyzed by the degree of fluorescence quenching. As shown in Fig. S28,† the fluorescence emission intensity of **MS-6T** at 469 nm decreased rapidly with the increase of fullerenes C_{60} and C_{70}, implying the formation of supramolecular complexes. Similarly, the fluorescence emission intensity of **MF-4T** at 504 nm was also quenched obviously when C_{60} and C_{70} were added to the solution. By fitting the data of multiple fluorescence titrations into different binding models (1 : 1 or 2 : 1) and analyzing the residual plots,[32] we found that for **MS-6T**, 2 : 1 is a more ideal stoichiometry (Fig. S28 and 29†), while for **MF-4T**, only the 1 : 1 model can obtain an effective binding constant, which proves that 1 : 1 may be a more appropriate stoichiometry. And the binding constants K_a and associated data of four macrocycles and fullerenes C_{60}/C_{70} were obtained by nonlinear fitting of fluorescence titration data, which have been detailed in Tables 1 and S6.†

To study the supramolecular assembly behaviors of macrocycles and fullerenes more directly, co-crystals of **MS-6T**@C_{60} and **MS-6T**@C_{70} were obtained by slow diffusion of methanol into a 2 : 1 mixture of **MS-6T** and C_{60} or C_{70} in toluene. The structures of these complexes were analyzed by single crystal XRD. As shown in Fig. 10, both C_{60} and C_{70} can bind well to the bowl-shaped macrocycle **MS-6T**. For co-crystals **MS-6T**@C_{60}, there is a molecule of C_{60} (purple) fully encapsulated in the large cavity of a capsule, which is composed of two **MS-6T**s through twelve C–H$\cdots\pi$ interactions (shown in Fig. 10a as black dashed lines) between the phenanthrene (Phen) and the conjugated framework of the outer rim of the other macrocycle **MS-6T** ($d_{C-H\cdots\pi}$ = 3.06 Å). And the supramolecular assembly is achieved by π–π interactions (shown in Fig. 10a as red dashed lines) between the spherical C_{60} and benzodithiophene (BDTh) units[33] at the inner edge of the bowl-shaped molecule **MS-6T** at a distance of 3.34 Å. Interestingly, in addition to the C_{60} located in the inner cavity of the molecular capsule, six other C_{60} molecules fill the outer part of the capsule through π–π interactions (shown in Fig. 10b as blue dashed lines) between the

Table 1 Binding constants of **MS-6T**/**MF-4T** and C_{60}/C_{70} (in toluene) along with the associated standard errors

	K_{11} [M^{-1}]	K_{21} [M^{-1}]
MS-6T@C_{60}	$(8.71 \pm 0.54) \times 10^5$	$(1.04 \pm 0.04) \times 10^5$
MS-6T@C_{70}	$(5.10 \pm 0.14) \times 10^5$	$(2.44 \pm 0.42) \times 10^5$
MF-4T@C_{60}	$(2.09 \pm 0.18) \times 10^4$	
MF-4T@C_{70}	$(1.62 \pm 0.25) \times 10^5$	

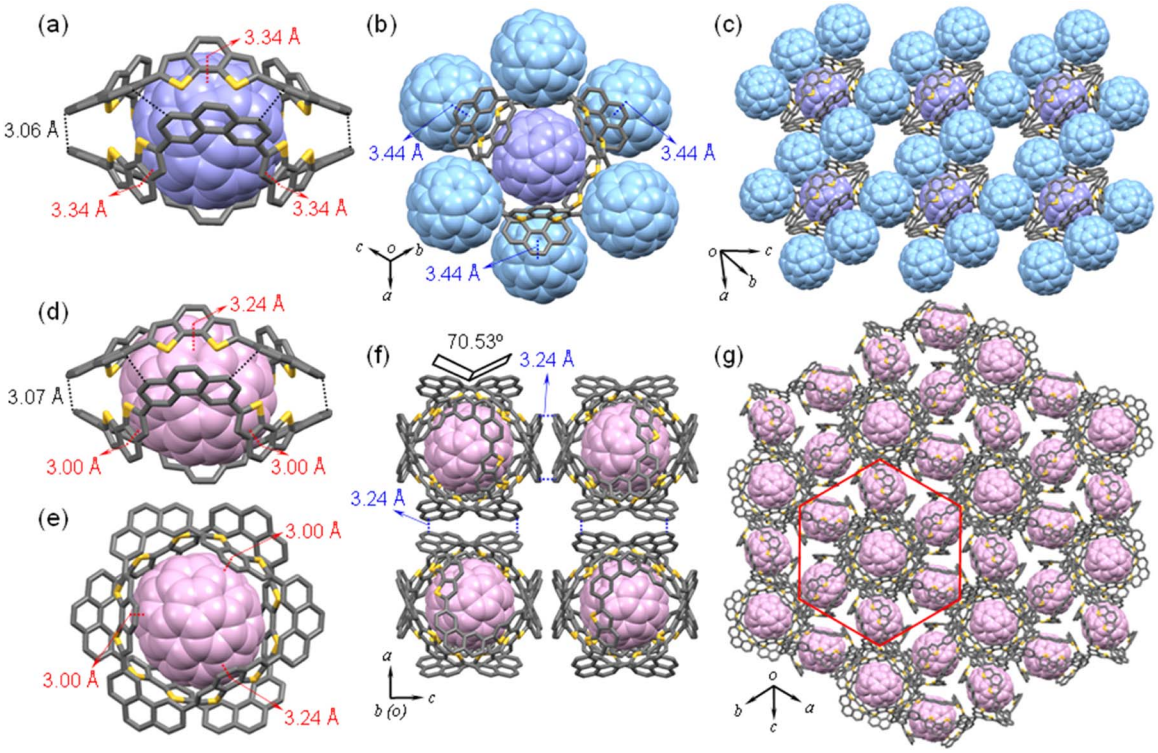

Fig. 10 X-ray crystallographic analysis of (a) side view of co-crystals **MS-6T**@C_{60}, (b) top view of co-crystals **MS-6T**@C_{60}, (c) 3D packing structures for **MS-6T**@C_{60}. (d) Side view of co-crystals **MS-6T**@C_{70}, (e) top view of co-crystals **MS-6T**@C_{70}, (f) 3D packing structure for eight sets of **MS-6T**@C_{70} molecular capsules in a unit cell, (g) the molecular packing arrangement of the honeycomb structure for **MS-6T**@C_{70}. The range of solid red lines is shown as the smallest constituent unit of the honeycomb lattice.

outer rim of **MS-6T** and spherical fullerenes with a distance of 3.44 Å, forming a symmetrical hexagonal arrangement. Analysis of the stacking pattern of **MS-6T**@C_{60} shows that there are multiple π–π interactions (Fig. 10c) between the six C_{60} molecules on the outside of one dimer capsule and neighboring capsules with a distance of 3.44 Å, which are conducive to the regular arrangement of co-crystal molecules in long-range space.

On the other hand, the crystal structure of **MS-6T**@C_{70} has also been thoroughly studied. Similar to **MS-6T**@C_{60}, the macrocycles in **MS-6T**@C_{70} also appear as capsules created by the dimerization of two **MS-6T**s through C–H···π interaction (shown in Fig. 10d as black dashed lines) between the phenanthrene (Phen) and the other macrocycle **MF-6T** ($d_{C-H\cdots\pi}$ = 3.07 Å), whose dimensions are identical to those of capsules in **MS-6T**@C_{60}. One ellipsoidal C_{70} resides in the center of the capsule by π–π interactions (shown in Fig. 10d and e as red dashed lines) between the C_{70} and benzodithiophene (BDTh) units of the bowl-shaped molecule **MS-6T**. Due to the larger ellipsoidal structure of C_{70}, the maximum distance of π–π interactions is 3.24 Å and the minimum is 3.00 Å, indicating a stronger supramolecular interaction between C_{70} and **MS-6T** than that between C_{60} and **MS-6T**. However, unlike **MS-6T**@C_{60}, fullerene C_{70} was not found outside the capsules. Further crystallographic analysis showed that there are eight co-crystal molecules in the cube cell (Fig. 10f), which are distributed on eight vertices of the cube, and the angle between the two adjacent molecules is 70.53°. In addition, the C–H···π interactions ($d_{C-H\cdots\pi}$ = 3.24 Å, shown in Fig. 10f as blue dashed lines) are formed between two adjacent molecular capsules through the phenanthrene (Phen) and the conjugated framework. And due to these molecular capsules rotating at different angles and balanced C–H···π interactions, **MS-6T**@C_{70} exhibits a particularly complex hexagonal windmill-shaped packing,[34] which can also be called a honeycomb[35] arrangement. In fact, although some honeycomb structures have been reported in polymers[36] or non-planar graphene,[37] self-assembled honeycomb lattices of supramolecular complexes with special molecular capsules structures are rare and we may be the first to report supramolecular honeycomb structures supported by explicit crystallographic data. As shown in Fig. 10g, six molecular capsules perpendicular to the central capsule are distributed around the central molecular capsule and rotate at the same angle, thus forming a set of hexagonal phases, which can be considered as the smallest unit to construct a honeycomb lattice. It is also worth noting that due to the inherent three-dimensional structure of the molecular capsules, **MS-6T**@C_{70} molecules can realize honeycomb stacking in other directions to form a complex three-dimensional honeycomb lattice.

Conclusions

In summary, single bond linked π-conjugated macrocycles with different sizes (**MS-4T** and **MS-6T**) and corresponding fully

fused heterocycloarenes (**MF-4T** and **MF-6T**) were successfully synthesized by effective macrocycle formation strategy and the periphery fusion strategy. X-ray crystallographic analysis and DFT calculations reveal that the geometric configurations of macrocycles have been greatly changed by the periphery fusion, in which the single bond linked π-conjugated macrocycle **MS-4T** presents a rigid and nearly planar geometry while the heterocycloarene **MF-4T** adopts a bowl-shaped structure and the larger size macrocycle **MS-6T** presents a bowl-shaped structure while the heterocycloarene **MF-6T** shows a saddle-shaped geometric configuration. In addition, all four macrocycles exhibited local aromatic properties. The conjugation length and geometric configuration of these macrocycles greatly affect their optical and electrochemical properties. Moreover, **MS-6T** and **MF-4T** exhibit special supramolecular assembly behaviours with spherical C_{60} and ellipsoidal C_{70}, which can be attributed to their suitable size and unique bowl configuration. Among them, **MS-6T** and fullerenes can form unique molecular capsules and different spatial arrangements. In particular, the 2 : 1 complex molecular capsule **MS-6T**@C_{70} shows a very special honeycomb packing in long-range space, which may be the first three-dimensional honeycomb lattice found in a supramolecular complex, giving insights into the development of novel host–guest systems based on bowl-shaped macrocycles.

Data availability

Synthetic procedures and characterization data of new compounds, X-ray crystallographic data, details of all characterization studies and theoretical calculations, and additional spectra have been provided in the ESI File.† CCDC 2272202, 2272207, 2327360 and 2272225 contain the supplementary crystallographic data for this paper.

Author contributions

X. L. conceived and supervised the project. D. A. contributed to all experiments, data analysis, and manuscript writing. R. Z. and J. Z. participated in the experimental operations and data analysis. T. W. contributed to manuscript revision. Y. Z., Y. L. and X. L. were responsible for funding acquisition and manuscript revision. All authors have approved the final version of the manuscript.

Conflicts of interest

There are no conflicts to declare.

Acknowledgements

This work was financially supported by the National Natural Science Foundation of China (22322502, 52073063 and 61890940), the National Key R&D Program of China (2023YFB3609000), the Natural Science Foundation of Shanghai (22ZR1405800 and 23ZR1405100), and the Program for Professor of Special Appointment (Eastern Scholar) at the Shanghai Institutions of Higher Learning. Thanks to crystallographer Pengfei Zhou from Beijing Zhongkebaice Technology Service Co. for his help in the analysis of the single crystal structure.

Notes and references

1 (*a*) S. Eisler, R. McDonald, G. R. Loppnow and R. R. Tykwinski, Structural, Vibrational, and Electronic Characteristics of Enyne Macrocycles as a Function of Ring Strain, *J. Am. Chem. Soc.*, 2000, **122**, 6917–6928; (*b*) J. Kromer, I. Rios-Carreras, G. Fuhrmann, C. Musch, M. Wunderlin, T. Debaerdemaeker, E. Mena-Osteritz and P. Bauerle, Synthesis of the first fully alpha-conjugated macrocyclic oligothiophenes: Cyclo[n]thiophenes with tunable cavities in the nanometer regime, *Angew. Chem., Int. Ed.*, 2000, **39**, 3481–3486; (*c*) V. Martí-Centelles, M. D. Pandey, M. I. Burguete and S. V. Luis, Macrocyclization Reactions: The Importance of Conformational, Configurational, and Template-Induced Preorganization, *Chem. Rev.*, 2015, **115**, 8736–8834; (*d*) B. Szyszko, M. J. Białek, E. Pacholska-Dudziak and L. Latos-Grażyński, Flexible Porphyrinoids, *Chem. Rev.*, 2017, **117**, 2839–2909.

2 (*a*) Q. Chen, M. T. Trinh, D. W. Paley, M. B. Preefer, H. Zhu, B. S. Fowler, X. Y. Zhu, M. L. Steigerwald and C. Nuckolls, Strain-Induced Stereoselective Formation of Blue-Emitting Cyclostilbenes, *J. Am. Chem. Soc.*, 2015, **137**, 12282–12288; (*b*) B. Zhang, M. T. Trinh, B. Fowler, M. Ball, Q. Xu, F. Ng, M. L. Steigerwald, X. Y. Zhu, C. Nuckolls and Y. Zhong, Rigid, Conjugated Macrocycles for High Performance Organic Photodetectors, *J. Am. Chem. Soc.*, 2016, **138**, 16426–16431; (*c*) Y. Yang, M. Chu and Q. Miao, From Phenanthrylene Butadiynylene Macrocycles to S-Heterocycloarenes, *Org. Lett.*, 2018, **20**, 4259–4262; (*d*) M. Ball, B. Zhang, Y. Zhong, B. Fowler, S. Xiao, F. Ng, M. Steigerwald and C. Nuckolls, Conjugated Macrocycles in Organic Electronics, *Acc. Chem. Res.*, 2019, **52**, 1068–1078; (*e*) N. Zhang, L. Yang, W. Li, J. Zhu, K. Chi, D. Chang, Y. Qiao, T. Wang, Y. Zhao, X. Lu and Y. Liu, Alkyl-Substituted N,S-Embedded Heterocycloarenes with a Planar Aromatic Configuration for Hosting Fullerenes and Organic Field-Effect Transistors, *J. Am. Chem. Soc.*, 2022, **144**, 21521–21529; (*f*) J. Liu, W. Hu and L. Jiang, Monolayer molecular crystals and devices, *Sci. Bull.*, 2023, **68**, 1474–1477.

3 (*a*) T. Kawase and H. Kurata, Ball-, Bowl-, and Belt-Shaped Conjugated Systems and Their Complexing Abilities: Exploration of the Concave−Convex π−π Interaction, *Chem. Rev.*, 2006, **106**, 5250–5273; (*b*) X. Lu, T. Y. Gopalakrishna, Y. Han, Y. Ni, Y. Zou and J. Wu, Bowl-Shaped Carbon Nanobelts Showing Size-Dependent Properties and Selective Encapsulation of C_{70}, *J. Am. Chem. Soc.*, 2019, **141**, 5934–5941; (*c*) Y. Ni, F. Gordillo-Gámez, M. Peña Alvarez, Z. Nan, Z. Li, S. Wu, Y. Han, J. Casado and J. Wu, A Chichibabin's Hydrocarbon-Based Molecular Cage: The Impact of Structural Rigidity on Dynamics,

Stability, and Electronic Properties, *J. Am. Chem. Soc.*, 2020, **142**, 12730–12742; (*d*) J. Wang, Y.-Y. Ju, K.-H. Low, Y.-Z. Tan and J. Liu, A Molecular Transformer: A π-Conjugated Macrocycle as an Adaptable Host, *Angew. Chem., Int. Ed.*, 2021, **60**, 11814–11818; (*e*) J. Zhu, W. Li, N. Zhang, D. An, Y. Zhao, X. Lu and Y. Liu, Size-dependent properties and unusual reactivity of novel nonplanar heterocycloarenes, *Chem. Sci.*, 2022, **13**, 11174–11182.

4 (*a*) V. Schroeder, S. Savagatrup, M. He, S. Lin and T. M. Swager, Carbon Nanotube Chemical Sensors, *Chem. Rev.*, 2019, **119**, 599–663; (*b*) D. T. McQuade, A. E. Pullen and T. M. Swager, Conjugated Polymer-Based Chemical Sensors, *Chem. Rev.*, 2000, **100**, 2537–2574; (*c*) X. Dong, X. Dai, G. Li, Y.-M. Zhang, X. Xu and Y. Liu, Conformationally Confined Emissive Cationic Macrocycle with Photocontrolled Organelle-Specific Translocation, *Adv. Sci.*, 2022, **9**, 2201962.

5 (*a*) H. Thakellapalli, S. Li, B. Farajidizaji, N. N. Baughman, N. G. Akhmedov, B. V. Popp and K. K. Wang, Synthesis and Properties of Conjugated Macrocycles Containing 2,7-Bis(2-thienyl)-9H-fluoren-9-one Units, *Org. Lett.*, 2017, **19**, 2674–2677; (*b*) K. Kato, Y. Kurakake, S. Ohtani, S. Fa, M. Gon, K. Tanaka and T. Ogoshi, Discrete Macrocycles with Fixed Chirality and Two Distinct Sides: Dipole-Dependent Chiroptical Response, *Angew. Chem., Int. Ed.*, 2022, **61**, e202209222; (*c*) W. Xu, Y. Nagata and N. Kumagai, TEtraQuinolines: A Missing Link in the Family of Porphyrinoid Macrocycles, *J. Am. Chem. Soc.*, 2023, **145**, 2609–2618.

6 (*a*) J. S. Reddy and V. G. Anand, Aromatic Expanded Isophlorins: Stable 30π Annulene Analogues with Diverse Structural Features, *J. Am. Chem. Soc.*, 2009, **131**, 15433–15439; (*b*) Y. Pareek, M. Ravikanth and T. K. Chandrashekar, Smaragdyrins: Emeralds of Expanded Porphyrin Family, *Acc. Chem. Res.*, 2012, **45**, 1801–1816; (*c*) L. Andreo, G. Volpi, F. Rossi, P. Benzi and E. Diana, Two-step Synthesis of a New Twenty-Membered Macrocycle: Spectroscopic Characterization and Theoretical Calculations, *ChemistrySelect*, 2022, **7**, e202202564.

7 (*a*) J. M. W. Chan, J. R. Tischler, S. E. Kooi, V. Bulović and T. M. Swager, Synthesis of J-Aggregating Dibenz[a,j] anthracene-Based Macrocycles, *J. Am. Chem. Soc.*, 2009, **131**, 5659–5666; (*b*) K. Miki, M. Fujita, Y. Inoue, Y. Senda, T. Kowada and K. Ohe, Synthesis of Strained Pyridine-Containing Cyclyne via Reductive Aromatization, *J. Org. Chem.*, 2010, **75**, 3537–3540.

8 (*a*) U. Beser, M. Kastler, A. Maghsoumi, M. Wagner, C. Castiglioni, M. Tommasini, A. Narita, X. Feng and K. Müllen, A C216-Nanographene Molecule with Defined Cavity as Extended Coronoid, *J. Am. Chem. Soc.*, 2016, **138**, 4322–4325; (*b*) G.-F. Huo, T. M. Fukunaga, X. Hou, Y. Han, W. Fan, S. Wu, H. Isobe and J. Wu, Facile Synthesis and Chiral Resolution of Expanded Helicenes with up to 35 cata-Fused Benzene Rings, *Angew. Chem., Int. Ed.*, 2023, **62**, e202218090.

9 (*a*) K. Ikemoto, A. Yoshii, T. Izumi, H. Taka, H. Kita, J. Y. Xue, R. Kobayashi, S. Sato and H. Isobe, Modular Synthesis of Aromatic Hydrocarbon Macrocycles for Simplified, Single-Layer Organic Light-Emitting Devices, *J. Org. Chem.*, 2016, **81**, 662–666; (*b*) K. Ikemoto, T. Tokuhira, A. Uetani, Y. Harabuchi, S. Sato, S. Maeda and H. Isobe, Fluorescence Enhancement of Aromatic Macrocycles by Lowering Excited Singlet State Energies, *J. Org. Chem.*, 2020, **85**, 150–157.

10 (*a*) F. Diederich and H. A. Staab, Benzenoid versus Annulenoid Aromaticity: Synthesis and Properties of Kekulene, *Angew. Chem., Int. Ed.*, 1978, **17**, 372–374; (*b*) C. Krieger, F. Diederich, D. Schweitzer and H. A. Staab, Molecular Structure and Spectroscopic Properties of Kekulene, *Angew. Chem., Int. Ed.*, 1979, **18**, 699–701; (*c*) H. A. Staab and F. Diederich, Cycloarenes, a New Class of Aromatic Compounds, I. Synthesis of Kekulene, *Chem. Ber.*, 1983, **116**, 3487–3503.

11 B. Kumar, R. L. Viboh, M. C. Bonifacio, W. B. Thompson, J. C. Buttrick, B. C. Westlake, M.-S. Kim, R. W. Zoellner, S. A. Varganov, P. Mörschel, J. Teteruk, M. U. Schmidt and B. T. King, Septulene: The Heptagonal Homologue of Kekulene, *Angew. Chem., Int. Ed.*, 2012, **51**, 12795–12800.

12 M. A. Majewski, Y. Hong, T. Lis, J. Gregoliński, P. J. Chmielewski, J. Cybińska, D. Kim and M. Stępień, Octulene: A Hyperbolic Molecular Belt that Binds Chloride Anions, *Angew. Chem., Int. Ed.*, 2016, **55**, 14072–14076.

13 H. Miyoshi, S. Nobusue, A. Shimizu and Y. Tobe, Non-alternant non-benzenoid kekulenes: the birth of a new kekulene family, *Chem. Soc. Rev.*, 2015, **44**, 6560–6577.

14 G. R. Newkome, J. D. Sauer, J. M. Roper and D. C. Hager, Construction of synthetic macrocyclic compounds possessing subheterocyclic rings, specifically pyridine, furan, and thiophene, *Chem. Rev.*, 1977, **77**, 513–597.

15 B. V. Phulwale, S. K. Mishra, M. Nečas and C. Mazal, Phenanthrylene-butadiynylene and Phenanthrylene-thienylene Macrocycles: Synthesis, Structure, and Properties, *J. Org. Chem.*, 2016, **81**, 6244–6252.

16 M. Kuritani, S. Tashiro and M. Shionoya, Heterodinuclear Metal Arrangement in a Flat Macrocycle with Two Chemically- Equivalent Metal Chelating Sites, *Inorg. Chem.*, 2012, **51**, 1508–1515.

17 M. Taniguchi and J. S. Lindsey, Synthetic Chlorins, Possible Surrogates for Chlorophylls, Prepared by Derivatization of Porphyrins, *Chem. Rev.*, 2017, **117**, 344–535.

18 (*a*) L. Zhang, J. Mu, Z. Jiang, H. Zhang and X. Yue, Fully aromatic macrocycle-terminated polyimide: synthesis and cross-linking, *Angew. Chem., Int. Ed.*, 2013, **24**, 415–420; (*b*) R. Inoue, M. Hasegawa, T. Nishinaga, K. Yoza and Y. Mazaki, Efficient Synthesis, Structure, and Complexation Studies of Electron-Donating Thiacalix[n] dithienothiophene, *Angew. Chem., Int. Ed.*, 2015, **54**, 2734–2738; (*c*) R. Kurosaki, H. Hayashi, M. Suzuki, J. Jiang, M. Hatanaka, N. Aratani and H. Yamada, A remarkably strained cyclopyrenylene trimer that undergoes metal-free direct oxygen insertion into the biaryl C–C σ-bond, *Chem. Sci.*, 2019, **10**, 6785–6790.

19 (*a*) A. Borissov, Y. K. Maurya, L. Moshniaha, W.-S. Wong, M. Żyła-Karwowska and M. Stępień, Recent Advances in Heterocyclic Nanographenes and Other Polycyclic

Heteroaromatic Compounds, *Chem. Rev.*, 2022, **122**, 565–788; (*b*) T. Luo, Y. Wang, J. Hao, P.-A. Chen, Y. Hu, B. Chen, J. Zhang, K. Yang and Z. Zeng, Furan-Extended Helical Rylenes with Fjord Edge Topology and Tunable Optoelectronic Properties, *Angew. Chem., Int. Ed.*, 2023, **62**, e202214653.

20 D. Myśliwiec and M. Stępień, The Fold-In Approach to Bowl-Shaped Aromatic Compounds: Synthesis of Chrysaoroles, *Angew. Chem., Int. Ed.*, 2013, **52**, 1713–1717.

21 J. Xie, X. Li, S. Wang, A. Li, L. Jiang and K. Zhu, Heteroatom-bridged molecular belts as containers, *Nat. Commun.*, 2020, **11**, 3348.

22 (*a*) H. Gregolińska, M. Majewski, P. J. Chmielewski, J. Gregoliński, A. Chien, J. Zhou, Y.-L. Wu, Y. J. Bae, M. R. Wasielewski, P. M. Zimmerman and M. Stępień, Fully Conjugated [4]Chrysaorene. Redox-Coupled Anion Binding in a Tetraradicaloid Macrocycle, *J. Am. Chem. Soc.*, 2018, **140**, 14474–14480; (*b*) Z. Luo, X. Yang, K. Cai, X. Fu, D. Zhang, Y. Ma and D. Zhao, Toward Möbius and Tubular Cyclopolyarene Nanorings via Arylbutadiyne Macrocycles, *Angew. Chem., Int. Ed.*, 2020, **59**, 14854–14860.

23 (*a*) X. Lu, T. Y. Gopalakrishna, H. Phan, T. S. Herng, Q. Jiang, C. Liu, G. Li, J. Ding and J. Wu, Global Aromaticity in Macrocyclic Cyclopenta-Fused Tetraphenanthrenylene Tetraradicaloid and Its Charged Species, *Angew. Chem., Int. Ed.*, 2018, **57**, 13052–13056; (*b*) B. Prajapati, D.-K. Dang, P. J. Chmielewski, M. A. Majewski, T. Lis, C. J. Gómez-García, P. M. Zimmerman and M. Stępień, An Open-Shell Coronoid with Hybrid Chichibabin–Schlenk Conjugation, *Angew. Chem., Int. Ed.*, 2021, **60**, 22496–22504.

24 N. M. O'boyle, A. L. Tenderholt and K. M. Langner, cclib: A library for package-independent computational chemistry algorithms, *J. Comput. Chem.*, 2008, **29**, 839–845.

25 W. Fan, Y. Han, X. Wang, X. Hou and J. Wu, Expanded Kekulenes, *J. Am. Chem. Soc.*, 2021, **143**, 13908–13916.

26 R. Dong, M. Pfeffermann, D. Skidin, F. Wang, Y. Fu, A. Narita, M. Tommasini, F. Moresco, G. Cuniberti, R. Berger, K. Müllen and X. Feng, Persulfurated Coronene: A New Generation of "Sulflower", *J. Am. Chem. Soc.*, 2017, **139**, 2168–2171.

27 (*a*) D. Geuenich, K. Hess, F. Köhler and R. Herges, Anisotropy of the Induced Current Density (ACID), a General Method To Quantify and Visualize Electronic Delocalization, *Chem. Rev.*, 2005, **105**, 3758–3772; (*b*) B. Li, C. Yang, X. Wang, G. Li, W. Peng, H. Xiao, S. Luo, S. Xie, J. Wu and Z. Zeng, Synthesis and Structural Elucidation of Bisdibenzocorannulene in Multiple Redox States, *Angew. Chem., Int. Ed.*, 2021, **60**, 19790–19796.

28 (*a*) Y. Ruiz-Morales, The Agreement between Clar Structures and Nucleus-Independent Chemical Shift Values in Pericondensed Benzenoid Polycyclic Aromatic Hydrocarbons: An Application of the Y-Rule, *J. Phys. Chem. A*, 2004, **108**, 10873–10896; (*b*) Z. Chen, C. S. Wannere, C. Corminboeuf, R. Puchta and P. v. R. Schleyer, Nucleus-Independent Chemical Shifts (NICS) as an Aromaticity Criterion, *Chem. Rev.*, 2005, **105**, 3842–3888.

29 P. Thordarson, Determining association constants from titration experiments in supramolecular chemistry, *Chem. Soc. Rev.*, 2011, **40**, 1305–1323.

30 Y. Tian, Y. Guo, X. Dong, X. Wan, K.-H. Cheng, R. Chang, S. Li, X. Cao, Y.-T. Chan and A. C. H. Sue, Synthesis of covalent organic pillars as molecular nanotubes with precise length, diameter and chirality, *Nat. Synth.*, 2023, **2**, 395–402.

31 Y. Shi, K. Cai, H. Xiao, Z. Liu, J. Zhou, D. Shen, Y. Qiu, Q.-H. Guo, C. Stern, M. R. Wasielewski, F. Diederich, W. A. Goddard III and J. F. Stoddart, Selective Extraction of C_{70} by a Tetragonal Prismatic Porphyrin Cage, *J. Am. Chem. Soc.*, 2018, **140**, 13835–13842.

32 (*a*) D. Brynn Hibbert and P. Thordarson, The death of the Job plot, transparency, open science and online tools, uncertainty estimation methods and other developments in supramolecular chemistry data analysis, *Chem. Commun.*, 2016, **52**, 12792–12805; (*b*) N. Grabicki, S. Fisher and O. Dumele, A Fourfold Gold(I)–Aryl Macrocycle with Hyperbolic Geometry and its Reductive Elimination to a Carbon Nanoring Host, *Angew. Chem., Int. Ed.*, 2023, **62**, e202217917; (*c*) K. Li, Z. Xu, H. Deng, Z. Zhou, Y. Dang and Z. Sun, Dimeric Cycloparaphenylenes with a Rigid Aromatic Linker, *Angew. Chem., Int. Ed.*, 2021, **60**, 7649–7653; (*d*) *Non-linear least-squares curve fitting were carried out with the online software Bindfit*. **http://supramolecular.org**.

33 H. Shimizu, J. D. Cojal González, M. Hasegawa, T. Nishinaga, T. Haque, M. Takase, H. Otani, J. P. Rabe and M. Iyoda, Synthesis, Structures, and Photophysical Properties of π-Expanded Oligothiophene 8-mers and Their Saturn-Like C60 Complexes, *J. Am. Chem. Soc.*, 2015, **137**, 3877–3885.

34 T. Nishikawa, H. Narita, S. Ogi, Y. Sato and S. Yamaguchi, Hydrophobicity and CH/π-interaction-driven self-assembly of amphiphilic aromatic hydrocarbons into nanosheets, *Chem. Commun.*, 2019, **55**, 14950–14953.

35 Z. Zhang, A. Kutana, Y. Yang, N. V. Krainyukova, E. S. Penev and B. I. Yakobson, Nanomechanics of carbon honeycomb cellular structures, *Carbon*, 2017, **113**, 26–32.

36 Q. Zhang, X. Yang, P. Li, G. Huang, S. Feng, C. Shen, B. Han, X. Zhang, F. Jin, F. Xu and T. J. Lu, Bioinspired engineering of honeycomb structure – Using nature to inspire human innovation, *Prog. Mater. Sci.*, 2015, **74**, 332–400.

37 D. Meng, G. Liu, C. Xiao, Y. Shi, L. Zhang, L. Jiang, K. K. Baldridge, Y. Li, J. S. Siegel and Z. Wang, Corannurylene Pentapetalae, *J. Am. Chem. Soc.*, 2019, **141**, 5402–5408.

38 (*a*) G. Portella, J. Poater and M. Solà, Assessment of Clar's aromatic π-sextet rule by means of PDI, NICS and HOMA indicators of local aromaticity, *J. Phys. Org. Chem.*, 2005, **18**, 785–791; (*b*) D. Jan Cz, Three Queries about the HOMA Index, *ACS Omega*, 2019, **4**, 18699–18710; (*c*) D. Jan Cz and O. Sławomir, HOMA Index Establishes Similarity to a Reference Molecule, *J. Chem. Inf. Model.*, 2023, **63**, 7744–7754.